Task 3.2

Title

Computational energy innovation

Projects (presented on the following pages)

GPU-SPHEROS: A GPU-Accelerated Versatile Solver Based on the Finite Volume Particle Method
S. Alimirzazadeh, E. Jahanbakhsh, A. Maertens, S. Leguizamon, F. Avellan

Efficient Finite Element Simulation Methods for Fracture Networks
M. Favino, J. Hunziker, K. Hollliger, R. Krause

Parallel Methods for Contact Problems in Rough Rock Surfaces
R. Krause, M. Nestola, D. Vogler, C. von Planta, P. Zulian

A Multiscale Model for the Simulation of Sediment Impact Erosion
S. Leguizamón, E. Jahanbakhsh, A. Maertens, S. Alimirzazadeh, F. Avellan

Surface tension modeling: wetting and contact angle hysteresis
A. Maertens, E. Jahanbakhsh, F. Avellan

Reactive flow patterns in fractured media
J. Mindel, T. Driesner

Fictitious Domain Method for 3D FSI Simulations of Turbines
M. Nestola, P. Zulian, R. Krause

Investigating transport processes in 3D fractured reservoirs
P. Schaedle, A. Ebigbo, M. O. Saar

Sloshing motion of a water free surface in a Francis turbine operating in condenser mode
E. Vagnoni, A. Favrel, L. Andolfatto, F. Avellan

CSMP++GEM for reactive transport modelling with solid solutions
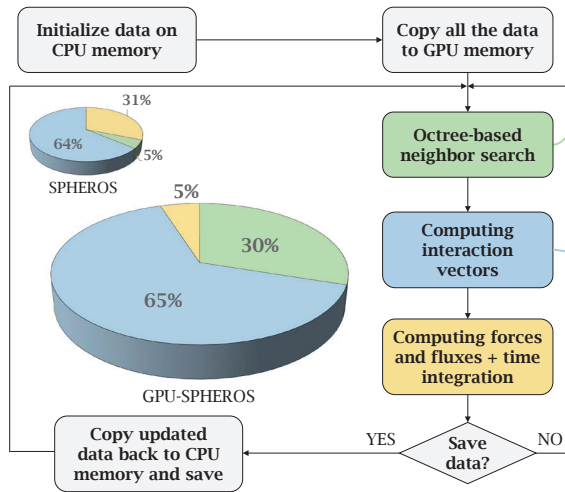A. Yapparova, G.D. Miron, D.A. Kulik, T. Driesner

SCCER-SoE Annual Conference 2016

SWISS COMPETENCE CENTER for ENERGY RESEARCH
SUPPLY of ELECTRICITY

LMH Laboratory for Hydraulic Machines

ÉCOLE POLYTECHNIQUE FÉDÉRALE DE LAUSANNE

In cooperation with the CTI

Energy
Swiss Competence Centers for Energy Research

Schweizerische Eidgenossenschaft
Confédération suisse
Confederazione Svizzera
Confederaziun svizra

Swiss Confederation

Commission for Technology and Innovation CTI

GPU-SPHEROS: A GPU-Accelerated Versatile Solver Based on the Finite Volume Particle Method

Siamak Alimirzazadeh, Ebrahim Jahanbakhsh, Audrey Maertens, Sebastián Leguizamón, François Avellan
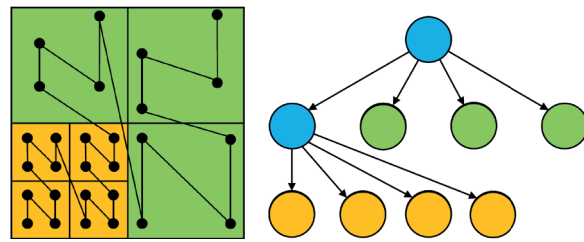
Introduction

GPU-SPHEROS is a **GPU-accelerated particle-based solver** based on Finite Volume Particle Method (**FVPM**) which inherits desirable features of both Smoothed Particle Hydrodynamics (SPH) and mesh-based Finite Volume Method (FVM) and is able to simulate the interaction between fluid, solid and silt [1]. With GPU-SPHEROS, the goal is to perform a industrial size setup simulations of hydraulic machines.

Software flowchart

Speedup

- On NVIDIA Tesla P100, GPU-SPHEROS is **5.5x faster** than the CPU version running on a node with 2 x Intel® Xeon® E5-2660 v2 and also more than 6x faster compared to one Intel Broadwell based machine with 2 x Intel® Xeon® E5-2690 v4 CPUs.
- Throughput reaches **3×10^5 particles per second** on Tesla P100.

Tesla K40 vs. Intel Xeon E5-2690v4
Tesla K40 vs. Intel Xeon E5-2660v2
Tesla P100 vs. Intel Xeon E5-2690v4
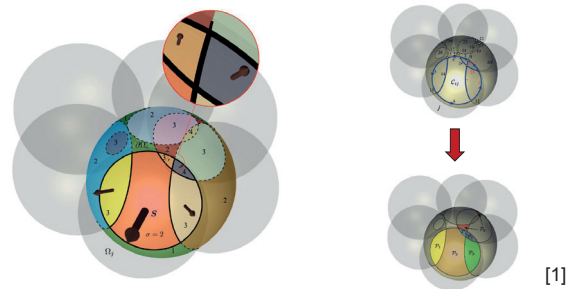Tesla P100 vs. Intel Xeon E5-2660v2

Octree-based neighbor search

- **Memory access efficiency** is a key point for GPU applications to be able to get a good performance.
- The data has been reordered using **space filling curves** (here, Morton curve) to improve memory access.
- An octree-based neighbor search algorithm has been implemented to find the neighbor particles.
- A highly optimized kernel has been implemented for parallel distance check between the particles.
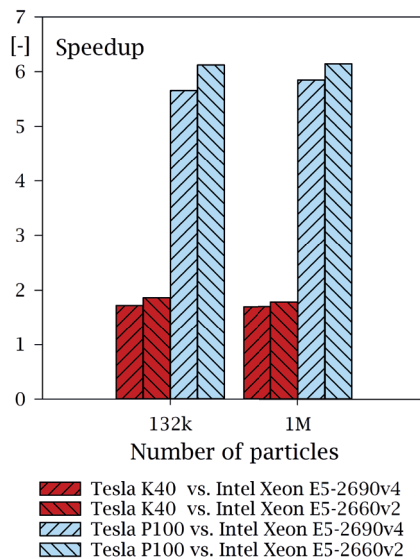

Computing interaction vectors

- FVPM can be interpreted as a generalization of conventional mesh-based FVM.
- In FVPM, control volumes are replaced by **overlapping particles** and the exchange occurs through the interfaces defined by overlapping regions.
- GPU-SPHEROS has been developed based on spherical-supported kernels.

[1]

Case study

- Fluid jet impinging on a flat plate
- The pressure coefficient has been compared to experimental data.
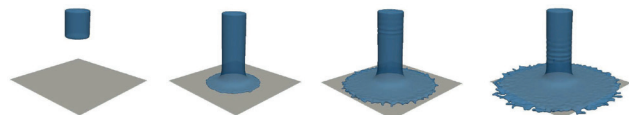
References

[1] E. Jahanbakhsh, A. Maertens, N. J. Quinlan, C. Vessaz, F. Avellan, Exact finite volume particle method with spherical-support kernels, *Comput. Methods Appl. Mech. Engrg.* 317 (2017) 102–127

SCCER-SoE Annual Conference 2017
Task 3.2: Computational Energy Innovation

Efficient Finite Element Simulation Methods for Fracture Networks

Marco Favino[1,2], Jürg Hunziker[2], Klaus Holliger[2], Rolf Krause[1]

[1]Institute of Computational Science, Università della Svizzera italiana
[2]Institute of Earth Sciences, University of Lausanne

Motivation

Numerical simulations of seismic waves in fractured rocks can result in significant advances for the indirect characterization of such environments. In fact, attenuation and modulus dispersion are due to fluid flow induced by pressure differences between regions of different compressibilities. Understanding these mechanisms in fractured rocks may provide information not only on fracture density but also on fracture connectivity. The main bottlenecks for these kinds of simulations are:

*   mesh generation; this requires human interaction to generate meshes which follow the geometry, thus making the simulation of realistic fracture networks unfeasible,
*   solution of the FE system due to its complicated structure, the large jumps in the material parameters, the complex nature of the variables in the frequency domain.

Methods

We developed a novel FE software called Parrot to study attenuation and modulus dispersion of seismic waves caused by fluid pressure diffusion in stochastic fracture networks. The new application has been developed inside the MOOSE framework. The latter has been extended in order to work with complex variables in order to simplify the form of the FE system and to speed-up the solution process when parallel direct solvers are employed. In Parrot, Biot's equation are solved in the time-frequency domain. The algorithm comprises the following steps:

1. Generation of a natural fracture networks, e.g. using a power-law distribution for fractures lengths
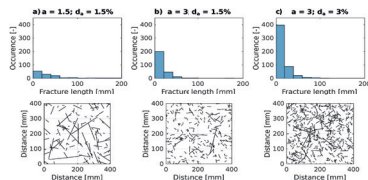

2. Adaptive mesh refinement (AMR) starting from a uniform coarse mesh
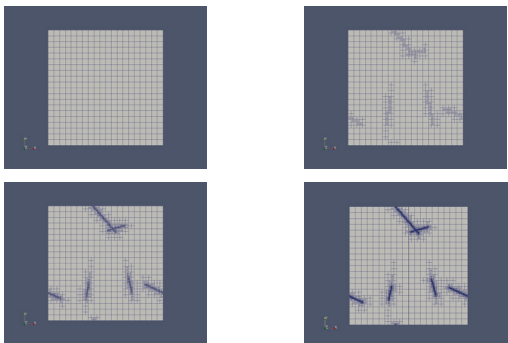
3. Solution of the linear system: the generated mesh is used to solve Biot's equations. The different levels can be employed in a multigrid solution process. The library MOONoLith allows for the parallel transfer between arbitrarily distributed meshes.
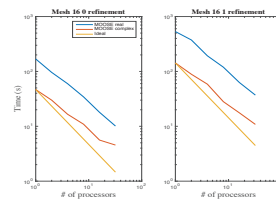
Validation

To show the effectiveness of our approach, we consider the problem of a spherically shaped inclusion. For this problem, an analytical solution has been provided by Pride et al. (2004). Starting from a coarse mesh 16x16x16, we applied 4 adaptive mesh refinement steps.
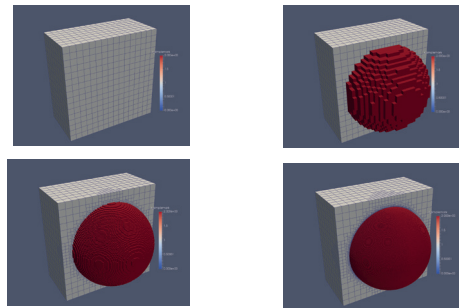
Convergence
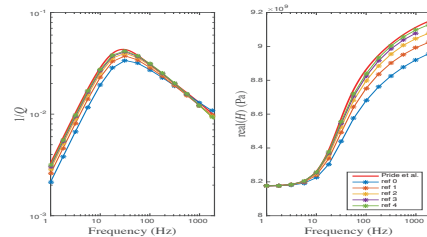
Scaling and speed-up

Discussion

The AMR approach allowed to reproduce the predicted attenuation and dispersion curves with a moderate number of unknowns (3M vs 135M of a uniform refinement approach). In particular, it confirmed the importance of having denser meshes at the interfaces where numerical inaccuracies are concentrated. The use of complex variables allowed to reduce the computational cost by a factor of 4 and the parallel direct solver MUMPS showed good scaling properties up to a moderate number of cores.

References

Biot, M. A., General theory for three-dimensional consolidation, Journal of Applied Physics, (1941), 12, 155–164.
Hunziker, J., Favino, M., Caspari, E., Quintal, B., Rubino, J. G., Krause, R., and Holliger, K., Seismic attenuation and modulus dispersion in porous rocks containing stochastic fracture networks, Journal of Geophysical Research (2017), under revision.
Pride, Berriman, Harris, Seismic attenuation due to wave-induced flow, Journal of Geophysical Research, (2004), vol. 109.

SCCER-SoE Annual Conference 2017
Task 3.2: Computational Energy Innovation

In cooperation with the CTI

Parallel Methods for Contact Problems in Rough Rock Surfaces

Rolf Krause[1], Maria Nestola[1], Daniel Vogler[2], Cyrill von Planta[1], Patrick Zulian[1]

[1]*Institute of Computational Science, Università della Svizzera italiana*
[2] *Institute of Geophysics ETH Zurich*

Earthquakes, Friction and Contact Problems

Earthquakes occur along pre-existing faults which start slipping when the effective normal stress falls below a certain threshold and the frictional strength between the two sides of the rock is below the shear stresses. Understanding the extent of the contact area is key to understanding the overall frictional behavior of rock fractures and to predict at which hydraulic pressures the two sides of a fault will start moving against each other.

Rough Rock Surfaces

We use high resolution photogrammetry scans from granitic samples of the Grimsel test site in Switzerland. We then add three dimensional bodies around the surfaces and generate FEM meshes with non-matching surfaces.
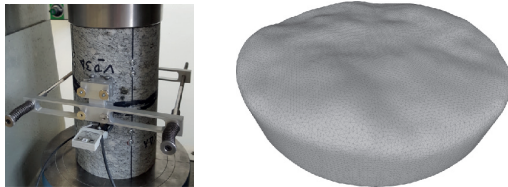

Figure: Left: Left: Rock sample with horizontal fracture in hydraulic press [3] Right: generated 3D mesh

Contact Formulation

$$-\operatorname{div}\sigma(\mathbf{u}) = f \quad in\ \Omega := \Omega_s \cup \Omega_m$$
$$\mathbf{u} = 0 \quad on\ \Gamma_D^n$$
$$\sigma_{ij}(\mathbf{u}) \cdot n_j = p_i \quad on\ \Gamma_N^n$$
$$\sigma_n \leq 0$$
$$[\mathbf{u} \cdot \mathbf{n}] = \mathbf{u}^s \cdot \mathbf{n}^s + \mathbf{u}^m \cdot \mathbf{n}^m$$
$$-\sigma(\mathbf{u}^m) = \sigma(\mathbf{u}^s)$$
$$[\mathbf{u} \cdot \mathbf{n}] \leq g$$
$$([\mathbf{u} \cdot \mathbf{n}] - g)\sigma_n = 0$$
$$\mathbf{u}_T = \mathbf{u} - u_n^a \cdot \mathbf{n}$$
$$[\mathbf{u}_T] = 0 \Rightarrow |\sigma_T| \leq \mathcal{F}|\sigma_n|$$
$$[\mathbf{u}_T] \neq 0 \Rightarrow \sigma_T = -\mathcal{F}|\sigma_n|\frac{[\mathbf{u}_T]}{|[\mathbf{u}_T]|}$$
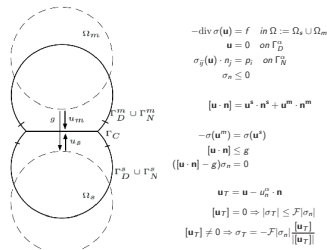
Figure: Strong formulation of frictional contact between two bodies.

We use a finite element formulation of linear elasticity. A mortar method is used to transfer the contact constraints between the contact surfaces. The resulting constrained linear system is solved with a semismooth newton or a nonsmooth multilevel method. The later has the advantage that it is of optimal complexity and extends multigrid efficiency to contact problems: it neither requires a regularization parameter nor multiple outer iterations.
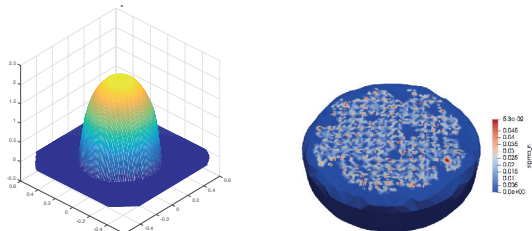

Figure: Left contact stresses for Hertzian contact. Right: contact stresses for rock sample.

Pseudo-L^2-Projections

To transfer the information from the contact boundary of one body to another and also for the Galerkin assembly of the nested multilevel hierarchy for the non-smooth multilevel method we use pseudo-L^2-projections.

$$T : V \longrightarrow W : \int_W (\mathbf{v} - T(\mathbf{v}))\,\mu\,d\omega = \int_W (\mathbf{v} - \mathbf{w})\,\mu\,d\omega = \mathbf{0}, \quad \forall \mu \in \mathbf{M}$$

Equation: The pseudo L^2-formulation **T** is defined in a weak sense whereby the multiplier space **M** consists of biorthogonal basis functions.
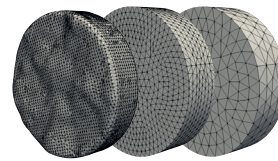

Figure: Multilevel hierarchy used for one body problem.

Implementation

For assembly of the finite element system we use MOOSE and for the solution of the system we use the PETSc SNES solver interface. The computation of the discrete L^2-projection carried out using libmesh and MOONoLith [1].
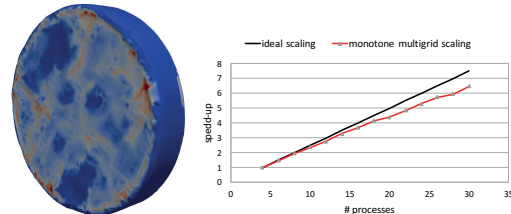
Results

Figure: Left: one-body contact problem. Right: Strong scaling experiment.

We computed one- and two-body frictionless contact problems, and, for benchmark purposes, cubes with up to 2.1 million degrees of freedom. The method scales well up to 30 processes which were the limit of our test environment.
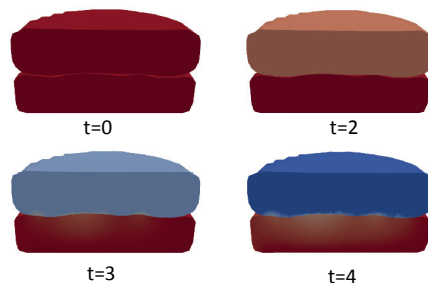

t=0   t=2
t=3   t=4

Figure: Cross section of the closing of two rocks in contact at timesteps t=0-4.

References
[1] Krause, Zulian SIAM 2016
[2] Dickopf, Krause Int. J. Numer. Meth. Engng 2008; 00:1–2
[3] Vogler, Settgast, Annavarapu, Madonna, Bayer and Amann, submitted

70 NRP   **Energy Turnaround**
National Research Programme

SCCER-SoE Annual Conference 2017

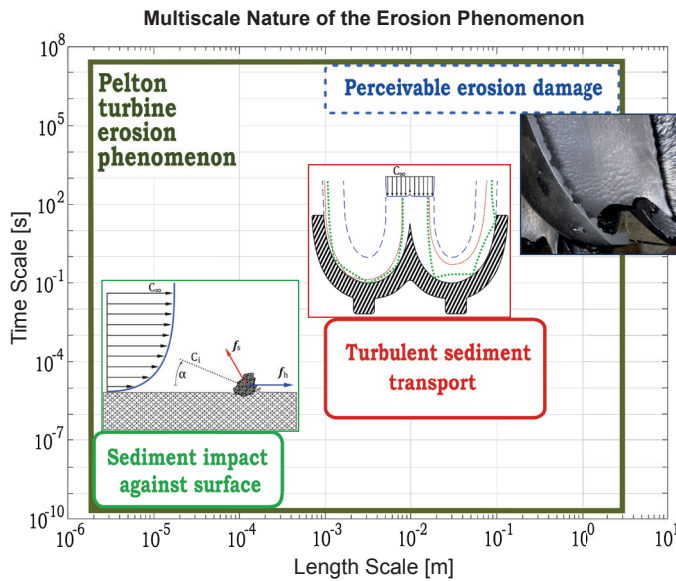# A Multiscale Model for the Simulation of Sediment Impact Erosion

Sebastián Leguizamón, Ebrahim Jahanbakhsh, Audrey Maertens, Siamak Alimirzazadeh, François Avellan

Motivation and Problem Description

The hydro-abrasive erosion of turbomachines is a **significant problem** worldwide. In the context of the Energy Strategy 2050, it is a problem which will become **more severe in the future** due to the retreat of glaciers and permafrost caused by **climate change**.

Our objective is to provide the **capability of simulating** the erosion process using the Finite Volume Particle Method [1]. Such simulations will become **advantageous** for both the **design** and the **operation** of the machines.

The erosion of hydraulic turbomachines is an **inherently multiscale process,** so its simulation is complicated. It demands a multiscale modeling approach.

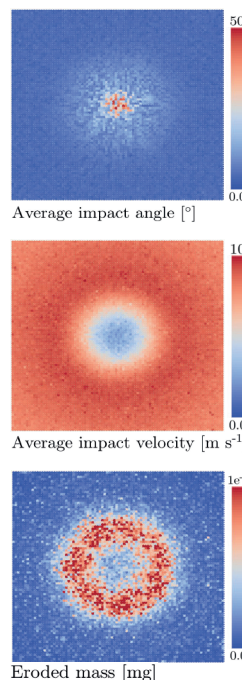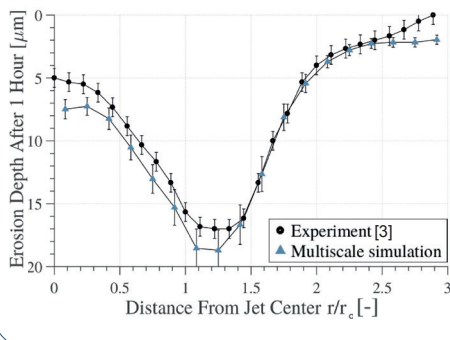**Multiscale Nature of the Erosion Phenomenon**

Multiscale Coupling and Validation

A sequential multiscale coupling algorithm is used to provide closure to the macroscale model based on the results of a finite set of microscale simulations.
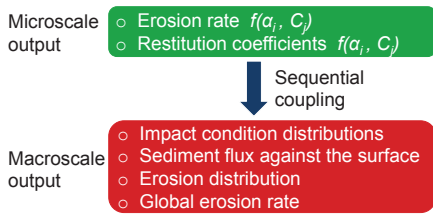
The slurry jet erosion of a flat plate is used to successfully validate the multiscale model.
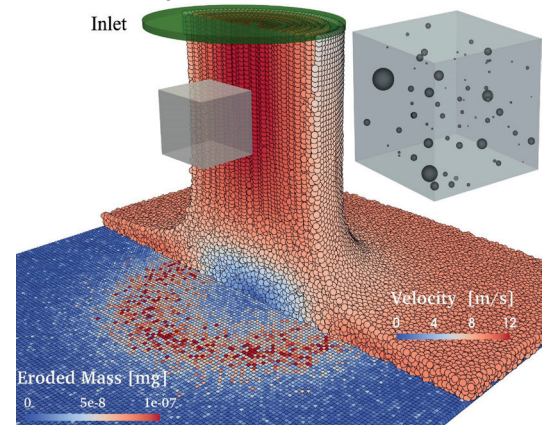

Macroscale Model: Sediment Transport

Turbulent sediment transport is computed in the macroscopic domain of interest.

o Finite Volume Particle Method
o Weakly compressible flow with k-ε turbulence closure
o Lagrangian sediment tracking accounting for drag, added mass, pressure gradient, turbulence dispersion, lift and interparticle contacts
o Arbitrary Weibull sediment size distribution at the inlet

**Slurry Jet Erosion of a Flat Plate**

Microscale Model: Sediment Impacts

Detailed thermomechanical modeling of the sediment collisions under constant impact conditions.

o Elastoplastic solid with the Johnson-Cook constitutive and damage models
o Thermoplastic and frictional heating
o Temperature-corrected Mie-Grüneisen equation of state
o Arbitrarily shaped elastic or rigid sediments

Spherical Particle Impacts against Solid
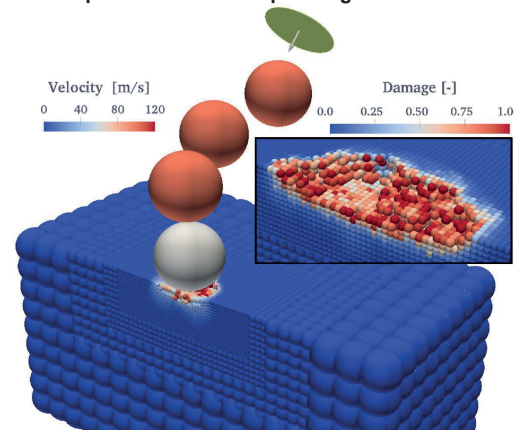
References

[1] E. Jahanbakhsh, A. Maertens, N. J. Quinlan, C. Vessaz, and F. Avellan, Exact finite volume particle method with spherical-support kernels, *Comput. Methods Appl. Mech. Engrg.*, 317: 02–127 (2017).
[2] K. Winkler, Understanding hydro-abrasive erosion for a sustainable future, *Hydro Vision India* (2011).
[3] K. Sugiyama, K. Harada, S. Hattori, Influence of impact angle of solid particles on erosion by slurry jet, *Wear* 265 (2008).

SCCER SoE

SWISS COMPETENCE CENTER for ENERGY RESEARCH
SUPPLY of ELECTRICITY

LMH Laboratory for Hydraulic Machines

EPFL
ÉCOLE POLYTECHNIQUE
FÉDÉRALE DE LAUSANNE

Surface tension modeling: wetting and contact angle hysteresis

Audrey Maertens, Ebrahim Jahanbakhsh, François Avellan

A versatile surface tension model for GPU-SPHEROS

- Finite Volume Particle Method $\Rightarrow$ each particle represents a physical volume of fluid [1]
- Approach: analytical particle interaction derived from macroscopic force on free surface for spherical fluid particles
- Surface tension force on particle i from free-surface (FS) elements $\mathcal{P}$ of surface area $S_\mathcal{P}$: $\boldsymbol{F}_i^{ST} = -\gamma \sum_{\mathcal{P} \in FS} \dfrac{\mathrm{d}S_\mathcal{P}}{\mathrm{d}\boldsymbol{x}_i}$.

air

fluid

Free surface in tension

Minimum free surface area $\Rightarrow$ No net force on i

- A 2 mm wide cubic water drop evolves into a ball under the action of the surface tension force

$t = 0$ $t = 1e\text{-}4\ s$ $t = 2e\text{-}4\ s$ $t = 3e\text{-}4\ s$ $t = 4e\text{-}4\ s$

$t = 8e\text{-}4\ s$ $t = 2.5e\text{-}3\ s$ $t = 5e\text{-}3\ s$ $t = \infty$

$\mathrm{d}S/\mathrm{d}\boldsymbol{x}_i$ [m]

Wetting

- Same approach in the presence of three interfaces: fluid-air ($\mathcal{I}_{FA}$), fluid-wall ($\mathcal{I}_{FW}$) and wall-air ($\mathcal{I}_{WA}$): $\boldsymbol{F}_i^{ST} = -\gamma_{FA} \sum_{\mathcal{P} \in \mathcal{I}_{FA}} \dfrac{\mathrm{d}S_\mathcal{P}}{\mathrm{d}\boldsymbol{x}_i} + (\gamma_{WA} - \gamma_{FW}) \sum_{\mathcal{P} \in \mathcal{I}_{FW}} \dfrac{\mathrm{d}S_\mathcal{P}}{\mathrm{d}\boldsymbol{x}_i}$
- Wettability is controlled by the equilibrium contact angle θ_e. Young's equation: $\gamma_{WA} - \gamma_{FW} = \gamma_{FA} \cos\theta_e = \gamma \cos\theta_e$

air

Hydrophilic:
$\gamma_{FW} < \gamma_{WA}$
$\cos\theta_e > 0$

fluid

wall

air

Hydrophobic:
$\gamma_{FW} > \gamma_{WA}$
$\cos\theta_e < 0$

fluid

wall
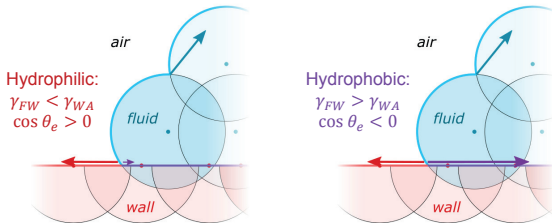
- Water drop shape on a flat surface and radius of wetted surface at equilibrium are a function of equilibrium contact angle

Normalized contact radius R_c^*

Hydrophilic

Hydrophobic

Equilibrium contact angle [°]

$\theta_e = 30°$ $\theta_e = 60°$ $\theta_e = 90°$ $\theta_e = 120°$ $\theta_e = 150°$

Contact angle hysteresis

- In dynamic cases, advancing angle $\neq$ receding angle
- Contact angle hysteresis largely due to imperfect wall surface
- Approach: directly model surface roughness rather than dynamic angle

- Procedure for each wall particle:
  1. Pick a random vector **V**
  2. Rotate particle about **V** by predefined ε

- Transforms a smooth surface into a surface of controlled roughness (here $\varepsilon = 0.1$ rad)

$\mathbf{n}_{W,s}^A$ $\mathbf{n}_{W,s}^B$ $\mathbf{n}_{W,s}^C$

$\mathbf{n}_{W,r}^A$ $\mathbf{n}_{W,r}^B$ $\mathbf{n}_{W,r}^C$

A B C   A B C

Flat surface   Rough surface

- The dynamics of a 3.6 mm diameter drop impacting a horizontal plane at 0.77 m/s is affected by contact angle hysteresis / surface roughness

Normalized contact radius R_c^*

$\theta_e = 87.4°$

- ∗ Experiment [2]
- Static contact angle [2]
- Model from Jiang et al. [2]
- SPHEROS rough surface
- SPHEROS smooth surface

Normalized time t^*

$t^* = 0.1$ $t^* = 0.25$ $t^* = 0.5$ $t^* = 0.8$ $t^* = 1.5$

Properties and applications

- A symmetric force directly derived from macroscopic interactions
  - Conservative
  - Stable
  - No model fitting or tuning needed
  - Versatile: can also handle surface roughness and contact angle hysteresis
- Energy applications
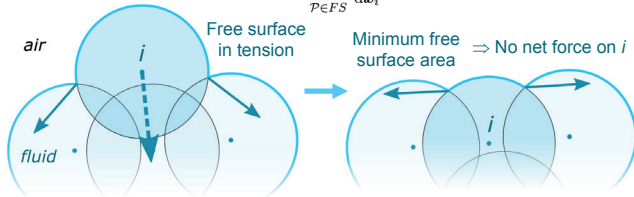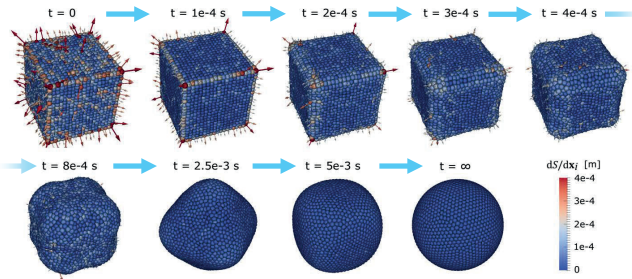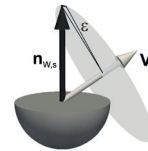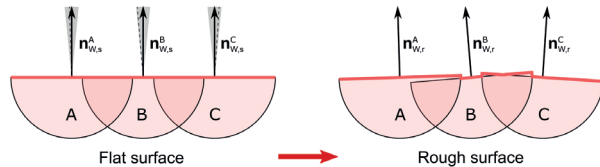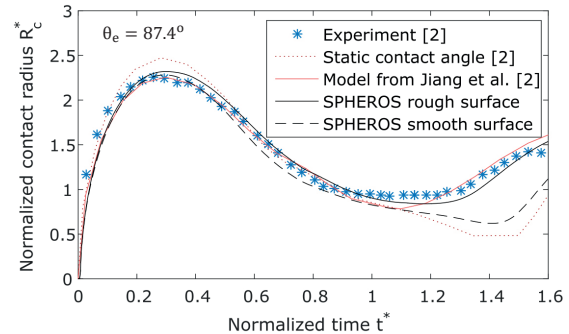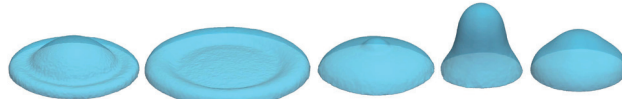 - Cavitation
  - Fracturing

References

[1] E. Jahanbakhsh, A. Maertens, N. J. Quinlan, C. Vessaz, and F. Avellan, "Exact finite volume particle method with spherical-support kernels," *Comput. Methods Appl. Mech. Engrg*., 317: 02–127, 2017.

[2] Y. Guo, Y. Lian, and M. Sussman, "Investigation of drop impact on dry and wet surfaces with consideration of surrounding air," *Phys. Fluids*, 28(7):073303, 2016.

SCCER-SoE Annual Conference 2017

Reactive flow patterns in fractured media

Julian Mindel and Thomas Driesner, Institute of Geochemistry and Petrology, ETH Zurich

In cooperation with the CTI

Abstract / Background

Reactive transport through irregularly fractured rock masses is a key phenomenon in ore-forming hydrothermal systems, geothermal systems, and many other geological processes. Assuming modelling of most other processes is already in place, the addition of RT as a simulation capability represents a steep increase in overall system complexity and computational expense.

Our approach to this problem includes a combination of the finite element and finite volume capabilities of our in-house CSMP++ flow simulation platform [1] with the GEMS3K [2] chemical equilibration code. Our current improvements include implementations in terms of OpenMP parallelism, heat transport, front end, and the creation of a higher-level modular re-usable code design.

Methodology & key progress

Through operator splitting and a sequential solution approach we assume conductive heat transfer to take place mainly through rock while advective heat transport happens in the fluid. The resulting thermal-compressive effects are coupled to mass transport via a *mass correction source term*s detailed in [5]. Figures 1 and 2 present sample test simulations in 2D, and 3D respectively.
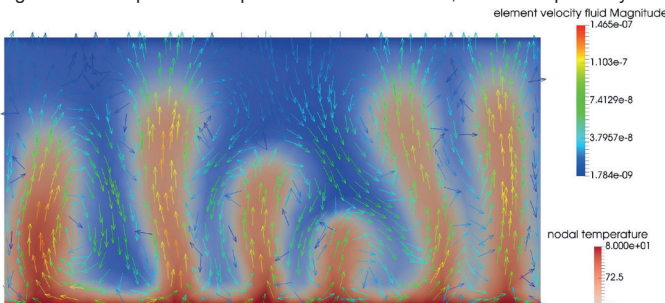

Figure 1: *Two dimensional test simulation of hydrothermal flow throw porous media. Heat is provided through the bottom boundary causing convective plumes to appear. Heat transport is modelled through the algorithm proposed in [5]*
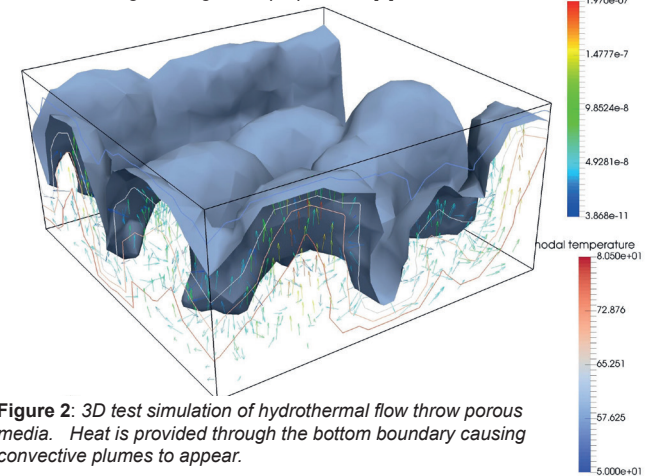

Figure 2: *3D test simulation of hydrothermal flow throw porous media. Heat is provided through the bottom boundary causing convective plumes to appear.*

Thin fractures and wells can be modelled via a lower-dimensional-element approach (LDE), allowing for complex networks that would otherwise incur prohibitive amounts of mesh resolution due to large scale differences. (Figure 3)
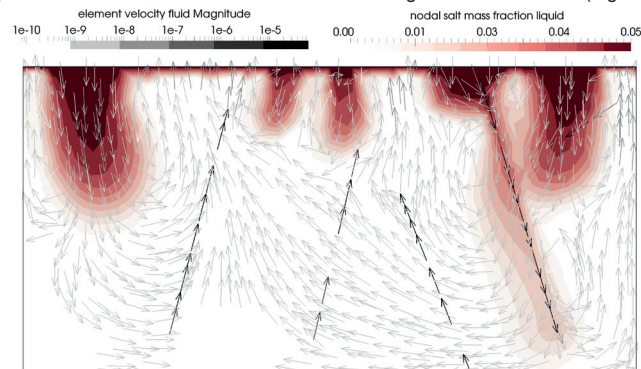

Figure 3: Salt fingers are caught in fracture flow (2D, triangular mesh). Higher flow velocities appear due to higher permeability assigned to line elements (LDEs) at the location of the fractures.

Honoring the governing equations for compressible porous media flow and chemical transport in our simulator, we also designed synthetic geometries (Figures 4 and 5) to study the propagation of a dolomitization front using the chemical conditions of the benchmark by Engesgaard and Kipp [3].

Conditions chosen in that benchmark minimize feedbacks resulting from porosity changes, etc.. The left sides of the simulation boxes are applied a Dirichlet boundary condition for aqueous Mg and a left to right pressure gradient is applied to induce flow.
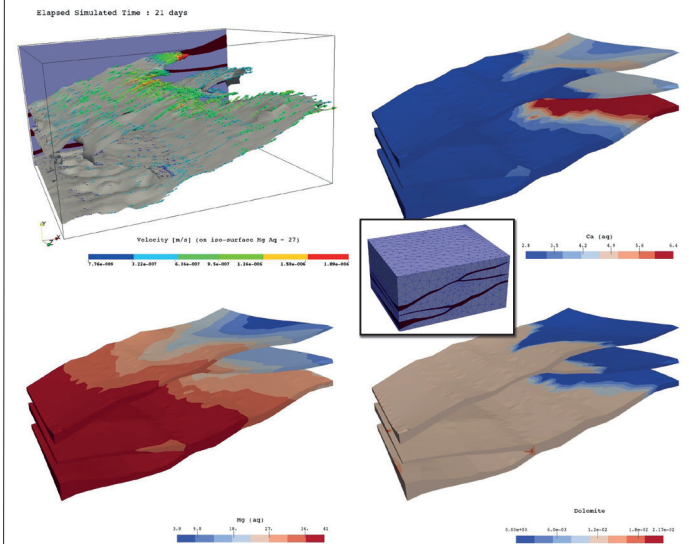

Figure 4 : In the model setup, calcite is considered to form a thin coating on pore walls and reacts to dolomite with the incoming aqueous Mg chloride solution. Due to thickness variations inside the fracture zones, their orientation in the fluid pressure field, and the effects of branching on fluid pressure gradients, the chemical front advances heterogeneously
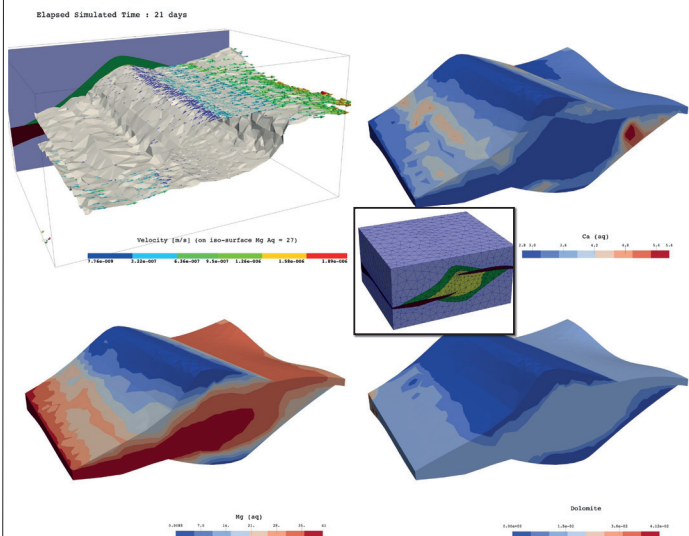

Figure 5: *Also here, non-uniformity of the geometry leads to heterogeneous advancement of the chemical front.*

Conclusions & Outlook

As sampled here, our approach is proving increasingly successful and is continuously tested on a variety of application problems. We are currently working towards adopting the CSMP++ "split node" approach [4] for reactive transport. Shifting focus on performance, we are also in the planning stages for CSMP++ native MPI functionality to be implemented and tested in combination with the GEMS library for simulations on distributed memory systems.

References

1. Matthai S.K. et al. (2012) ECMOR XIII, European Conf. Mathematics of Oil Recovery, Biarritz, France;
2. Kulik D.A. et al. (2013) Computational Geosciences 17,1-24; 3
3. Engesgaard, P., Kipp, K.L. (1992) Water Resour. Res. 28, 2829–2843; 4
4. Nick H.M. and Matthai S.K. (2011) Vadose Zone Journal 299-312
5. Weiss, P. et al. (2014) Geofluids 14, 347-371, 3

Fictitious Domain Method for 3D FSI Simulations of Turbines

Maria Giuseppina Chiara Nestola, Patrick Zulian, Rolf Krause

Institute of Computational Science, Università della Svizzera Italiana

Motivation

We present a completely parallel approach for Fluid-Structure Interaction (FSI) simulations.

Our approach is inspired by the fictitious domain method [1] and makes intensive use of variational transfer between the solid and the fluid grid.

For validation and evaluation of the accuracy of the proposed methodology, we present results for a benchmark configuration describing the deformations of two elastic beams in a flow channel.

We simulate the flow around a vertical axis turbine in order to show that the framework is suitable for industrial applications.

Mathematical Formulation

Find $(\mathbf{u}_f, p_f; \boldsymbol{\eta}_s, p_s; \boldsymbol{\lambda}) \subset (V_f \times Q_f \times V_s \times Q_s \times L)$ such that for every $(\mathbf{v}_f, q_f; \mathbf{v}_s, q_s; \boldsymbol{\mu}) \subset (V_f \times Q_f \times V_s \times Q_s \times L)$

$$\int_{\Omega_f} \rho_f \frac{\partial \mathbf{u}_f}{\partial t} \cdot \mathbf{v}_f \, dV + \int_{\Omega_f} \rho_f [(\mathbf{u}_f \cdot \nabla)\mathbf{u}_f] \cdot \mathbf{v}_f \, dV + \int_{\Omega_f} \sigma(\mathbf{u}_f, p_f) : \nabla \mathbf{v}_f \, dV - \int_{\mathscr{I}} \boldsymbol{\lambda} \cdot \mathbf{u}_f \, dV = 0$$
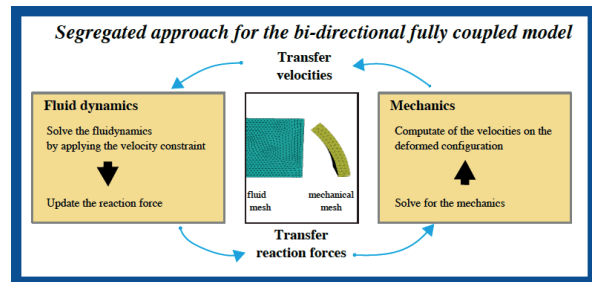
$$\int_{\Omega_f} q_f \nabla \cdot \mathbf{u}_f \, dV = 0$$

$$\int_{\mathscr{I}} \boldsymbol{\mu} \cdot \left(\frac{\partial \boldsymbol{\eta}_s}{\partial t} - \mathbf{u}_f \right) dV = 0$$

$$\int_{\widehat{\Omega}_s} \widehat{\rho}_s \frac{\partial^2 \widehat{\boldsymbol{\eta}}_s}{\partial t^2} \cdot \widehat{\mathbf{v}}_s \, dV + \int_{\widehat{\Omega}_s} \widehat{\mathbf{P}}(\widehat{\mathbf{F}}) : \nabla \widehat{\mathbf{v}}_s \, dV - \int_{\widehat{\Omega}_s} \widehat{p}_s \widehat{J} \widehat{\mathbf{F}}^{-T} : \nabla \widehat{\mathbf{v}}_s \, dV + \int_{\mathscr{I}} \boldsymbol{\lambda} \cdot \widehat{\mathbf{v}}_s \, dV = 0$$

$$\int_{\widehat{\Omega}_s} (\widehat{J} - 1) q_s \, dV = 0$$

$\widehat{\Omega}_s$: solid domain, Ω_f: fluid domain $\mathscr{I} := \widehat{\Omega}_s \cap \Omega_f$.

Segregated approach for the bi-directional fully coupled model

Transfer velocities

Fluid dynamics
Solve the fluidynamics by applying the velocity constraint

Update the reaction force

fluid mesh   mechanical mesh

Mechanics
Compute of the velocities on the deformed configuration

Solve for the mechanics

Transfer reaction forces

Coupling

- For coupling the fluid and the solid subproblems we adopt an inherently parallel approach for dealing with the L^2-projection operator. This approach includes a parallel search strategy, the computation of element intersections, and the parallel assembling of the transfer operator [2].
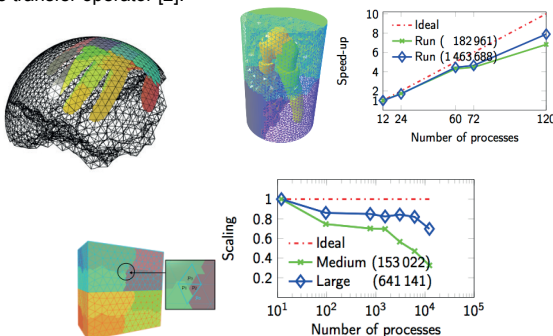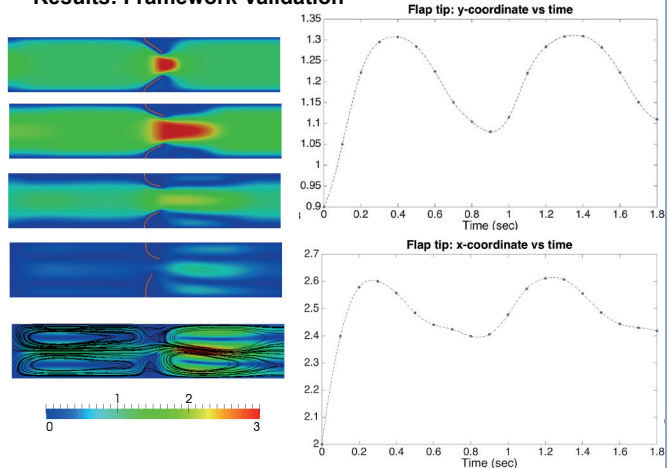

Results: Turbines Simulation
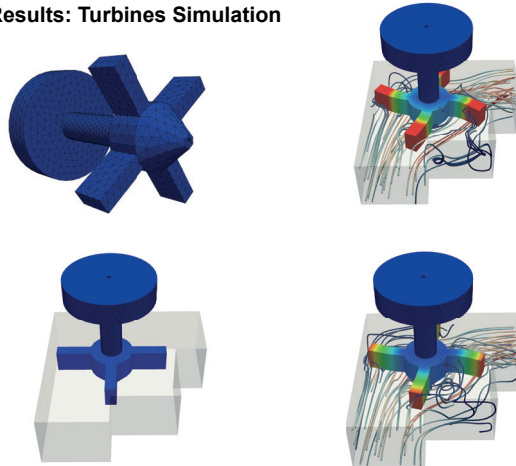
70 NRP **Energy Turnaround**
National Research Programme

Results: Framework Validation

Flap tip: y-coordinate vs time

Flap tip: x-coordinate vs time

Discussion

We validate the framework by using a benchmark consisting of two nonlinear elastic flapping beams embedded into a two-dimensional Newtonian flow-channel. By analysing the displacement field of a point placed on the top beam, we get results in agreement with Gil [3].

The FSI framework is employed for simulating a cross-flow vertical-axis water turbine. More specifically, we use a linear elastic material for simulating the turbine blades, whereas the water is modelled as a Newtonian flow with a moderate high Reynolds number (~2000).

References

[1] Frank P T Baaijens. *International Journal for Numerical Methods in Fluids*, 35(7):743–761, 2001.

[2] Rolf Krause and Patrick Zulian. *SIAM Journal on Scientific Computing*, 38(3):C307–C333, 2016.

[3] Gil, Antonio J., et al. *Journal of Computational Physics* 229.22 (2010): 8613-8641.

SCCER SoE

SWISS COMPETENCE CENTER for ENERGY RESEARCH
SUPPLY of ELECTRICITY

ETH *zürich*

In cooperation with the CTI

Energy
Swiss Competence Centers for Energy Research

Schweizerische Eidgenossenschaft
Confédération suisse
Confederazione Svizzera
Confederaziun svizra

Swiss Confederation

Commission for Technology and Innovation CTI

GEO
Geothermal Energy & Geofluids

Investigating transport processes in 3D fractured reservoirs

Philipp Schädle, Anozie Ebigbo, Martin O. Saar
ETH Zurich, Zurich, Switzerland

Introduction

- Two key aspects are relevant for sufficient energy production from enhanced geothermal systems:
  1. Sufficiently high fluid production rates.
  2. Maximum effective **fracture surface area**.
- Flow and transport behavior in 3D fracture networks strongly depends on **network-scale** and **fracture-scale heterogeneities** [1,2].
- This work presents:
  1. Simulations of fluid flow and particle transport through **discrete fracture networks (DFNs)**.
  2. The influence of network-scale heterogeneity on transport and effective fracture surface area.

Conceptual model

DFN

- Domain size: 10 x 10 x 10 m
- Fracture orientation: Random
- Fracture size distribution: **Truncated power law**
- Length correlated aperture
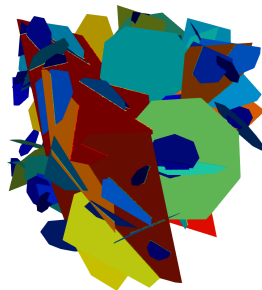- Aperture - permeability relation: Cubic law

Figure: Example of a discrete fracture network; colors show the fracture permeability

Fluid flow simulation

- **Steady-state** flow
- Pressure difference between two Dirichlet boundaries: 0.01 MPa

Particle transport simulation

- A **Lagrangian** approach is used to calculate particle transport through the network.
- Particles are injected at high pressure boundary and exit at low pressure boundary.
- Particles are **instantaneously** injected at all fractures which intersect the domain boundary.
- At **each fracture** which intersects the domain boundary an **equal amount** of particles are equidistantly injected.

Effective surface area

Network-scale heterogeneity leads to preferential pathways for fluid flow and transport. Hence, the effective surface area depends on the network-scale heterogeneity.
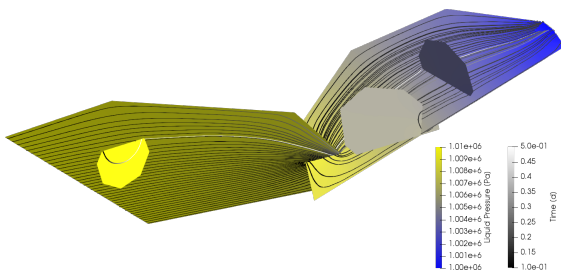

Figure: Pressure in fracture network consisting of five fractures. Trajectories of 40 particles with travel time [d]

The following observations can be made:

- **Dead-end fractures** are less affected by flow and transport.
- Particle transport is **delayed** by transport through hydraulically less transmissive fractures.
- Major parts of the particles are transported on **preferential pathways**.

Methods

Simulations are performed using *DFNworks* [3]. *DFNworks* is a code framework which allows to generate DFNs and model steady-state flow and particle transport. *PFLOTRAN* [4] is used to solve the flow part.

Calculation of the effective surface area

- Percentage of fracture surface area which is affected by transport.
- Calculated based on the grid cells of the DFN mesh.
- Grid cell is considered to be affected by transport, if:
  - a minimum of **n percent of all particles** is transported through the cell,
  - the particles intersecting the cell are not within the 10% particles with the largest travel time.

Preliminary Results

Two experiments have been performed:

1. Variing number of particles are injected in a single DFN.
2. Five different DFNs are generated based on equal network parameters. For each DFN, particle transport is simulated with 500 particles injected at each fracture.

For the two experiments the effective surface area is calculated for different percentage of considered particles.
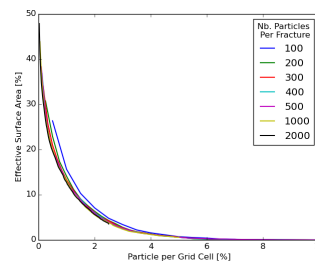

Figure: Effective surface area vs. percentage of considered particles. Different cases with varying number of injected particles at each fracture.
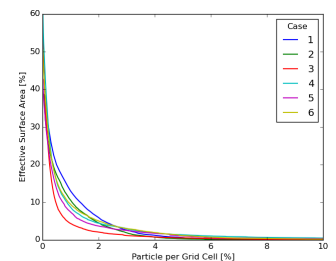

Figure: Effective surface area vs. percentage of considered particles. Realization of different DFNs with equal parameters. Injection of 500 particles per fracture

- The maximum effective surface area depends on the total number of injected particles.
- A minimum number of injected particles per grid cell at the domain boundary is required to calculate the effective surface area.
- If 1% of the particles are considered the effective surface area varies only over 2-3%, if a single DFN is considered.

Outlook

- Make stochastic investigations for multiple fracture network parameters.
- Investigate the influence of in-fracture variability on the effective surface area.
- Compare results for the effective surface area to borehole analysis methods.
- Investigate the influence of effective surface area on heat extraction rates.

References

1. de Dreuzy, J.-R., Meheust, Y., and Pichot, G. (2012). Influence of fracture scale heterogeneity on the flow properties of three-dimensional discrete fracture networks (DFN). Journal of Geophysical Research: Solid Earth, 117(B11):1-21.
2. Makedonska, N., Hyman, J. D., Karra, S., Painter, S. L., Gable, C. W., and Viswanathan, H. S. (2016). Evaluating the effect of internal aperture variability on transport in kilometer scale discrete fracture networks. Advances in Water Resources , 94(4):486-497.
3. Hyman, J.D., Karra, S., Makedinska, N., Gable, C.W., Painter, S.L., Viswanatha, H. (2015), dfnWorks: a discrete fracture network framework for modeling subsurface flow and transport. Computers & Geosciences, 84, pp. 10-19.
4. Lichtner, C.P., Hammond, G.E., Lu, C., Karra, S., Bisht, G., Andre, B., Mills, R.T., Kumar, J., Frederick, J.M., (2017). *PFLOTRAN* User Manual. http://www.documentation.pflotran.org

SCCER-SoE Annual Conference 2017

Sloshing motion of a water free surface in a Francis turbine operating in condenser mode

E. Vagnoni, A. Favrel, L. Andolfatto and F. Avellan

SCCER S SoE
SWISS COMPETENCE CENTER for ENERGY RESEARCH
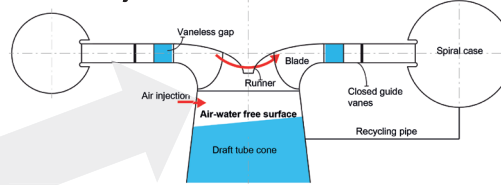SUPPLY of ELECTRICITY

In cooperation with the CTI
Energy
Swiss Competence Centers for Energy Research
Schweizerische Eidgenossenschaft
Confédération suisse
Confederazione Svizzera
Confederaziun svizra
Swiss Confederation
Commission for Technology and Innovation CTI
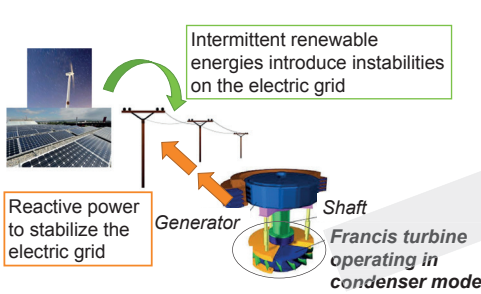
Context and objectives

Intermittent renewable energies introduce instabilities on the electric grid

Reactive power to stabilize the electric grid

Generator *Shaft*
Francis turbine operating in condenser mode

Vaneless gap
Blade
Runner
Air injection
Air-water free surface
Draft tube cone
Closed guide vanes
Spiral case
Recycling pipe

In condenser mode operation:
Turbine spins in air to minimize the power consumption: compressed air is injected in the draft tube cone → **Air losses recorded**

Research objectives:
- *Study of the air-water interaction phenomena.*
- *Focus on the sloshing motion of the free surface in the draft tube cone.*
- *Relation between the sloshing motion and the air losses.*

Experimental set-up

Reduced scale physical model

Cooling discharge
C2
Camera
White LED backlight
Air injection
C1
Wall pressure measurements
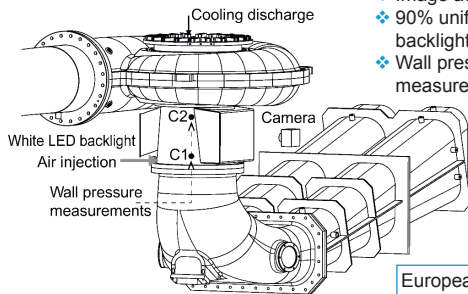
- ❖ Image acquisition at 30 Hz.
- ❖ 90% uniform white LED backlight.
- ❖ Wall pressure measurements at 3000 Hz.

Scaling law: $Fr_d = \sqrt{\dfrac{\rho_{air}}{\rho_{water}}} \dfrac{N\sqrt{D_e}}{\sqrt{g}}$

European project in collaboration with BC-Hydro for investigating two-phase flow phenomena affecting turbine performance

Methodology

Post-processing image method to evaluate the difference in elevation h of two sides of the free surface by image filtering and contrast detection
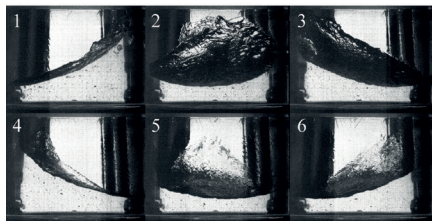
F(j,i)   E(j,i)
A B
C D
Selected matrices of pixels E(j,i) and F(j,i) for sloshing detection
y
x
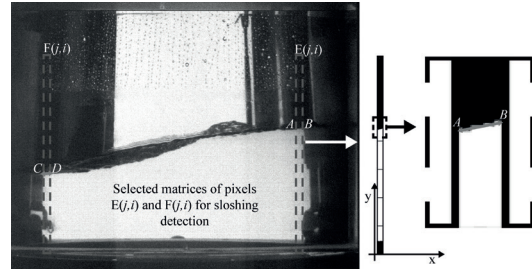
$y_{AB,i} = \sum_j \left(E(j,i) = 255 \right)$

$y_{CD,i} = \sum_j \left(F(j,i) = 255 \right)$

Linear interpolation

$y_B = ax_B + b$
$y_C = cx_C + d$

→ $h = y_B - y_C$

Results

Study of the sloshing motion in time and frequency domain

1 2 3
4 5 6
(a)

a. **Sequence of images** of the air-water oscillating free surface.
b. **Time resolved signals** of h.
c. **Corresponding spectrum magnitude.**

$h_{peak,i}$
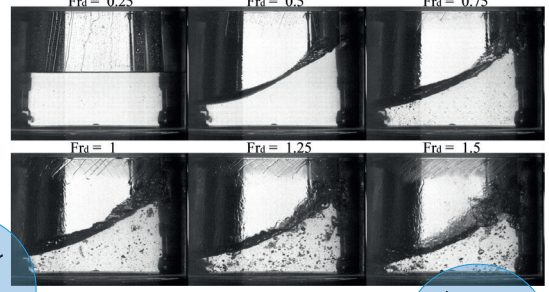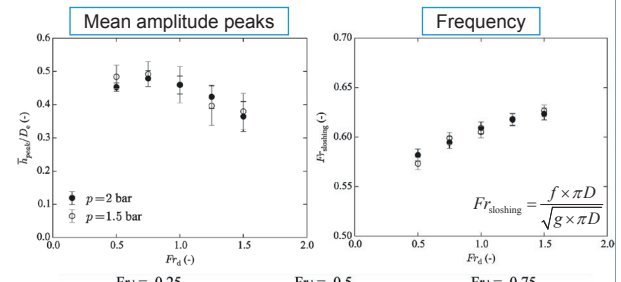
(b) t (s) h/D_e (-)

(c) $|h/D_e|$ (-) f (Hz)
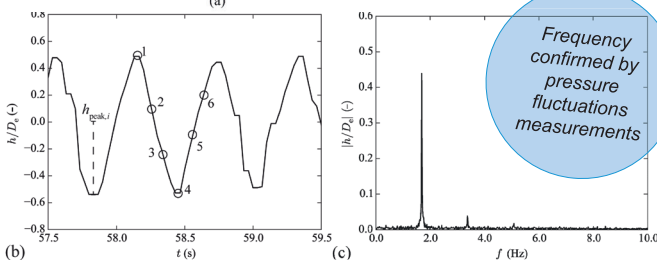
Frequency confirmed by pressure fluctuations measurements

Resonance gravity wave excited at the first natural frequency of the water volume in the draft tube cone

□ natural frequency
● sloshing frequency
f (Hz)
l/D (-)

Dependency of the sloshing amplitude and frequency by the densimetric Froude number

Mean amplitude peaks
$\bar{h}_{peak}/D_e$ (-)
Fr_d (-)
● $p = 2$ bar
○ $p = 1.5$ bar

Frequency
$Fr_{sloshing}$ (-)
Fr_d (-)

$Fr_{sloshing} = \dfrac{f \times \pi D}{\sqrt{g \times \pi D}}$

Fr_d = 0.25   Fr_d = 0.5   Fr_d = 0.75
Fr_d = 1   Fr_d = 1.25   Fr_d = 1.5

Fr_d key parameter of the sloshing motion

Increasing air-water mixing with Fr_d

E. Vagnoni et al., "Experimental investigation of the sloshing motion of the free surface in the draft tube of a Francis turbine operating in synchronous condenser mode", Experiments in Fluids (Submitted)

LMH *Laboratory for Hydraulic Machines*

EPFL
ÉCOLE POLYTECHNIQUE
FÉDÉRALE DE LAUSANNE

SCCER-SoE Annual Conference 2017

CSMP++GEM for reactive transport modelling with solid solutions

A. Yapparova (ETHZ), G.D. Miron (PSI), D.A. Kulik (PSI), T. Driesner (ETHZ)

Motivation

- Reactive transport models (RTM) with non-ideal multicomponent solid solutions and mixed gaseous fluids are necessary for modelling natural magmatic-hydrothermal and geothermal systems

- Widely used LMA (law of mass action) codes (e.g. TOUGHREACT, PHREEQC) cannot model such chemical systems efficiently

- Feldspars are among the most abundant minerals in the Earth's crust. Alkali feldspar is a non-ideal ternary solid solution with end members K-feldspar, Albite, Anortite and a miscibility gap

Methods

The CSMP++GEM reactive transport code:

- Control volume finite element method (CVFEM) to solve PDEs for two-phase flow and heat transport in terms of pressure, enthalpy and salinity on unstructured grids (Weis et al., 2014).

- Accurate thermodynamic representation of fluid properties – Equation of state for a H2O-NaCl system (Driesner&Heinrich, 2007; Driesner, 2007).

- Chemical equilibrium calculations using the Gibbs energy minimisation method (GEM), implemented within the GEMS3K code (Kulik et al.,2013; Wagner et al., 2012).

- Sequential Non-Iterative Approach (SNIA) for transport-chemistry coupling for fast reactive transport calculations (compared to SIA and fully implicit methods).

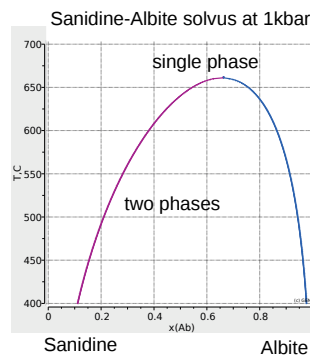## Alkali Feldspar solid solution with non-ideal mixing

3 end-members:
- Albite (Na)
- Sanidine (K)
- Anorthite (Ca)

Multi-component Van Laar model (Holland & Powell, 2003) describes the mixing properties in an asymmetric system:

- one binary interaction parameter per pair of end-members,

- one scaling parameter (size parameter) per end-member.

Sanidine-Albite solvus at 1kbar

implemented in **TsolMod library** (Wagner et al., 2012)

1D model setup: Albitisation of K-feldspar

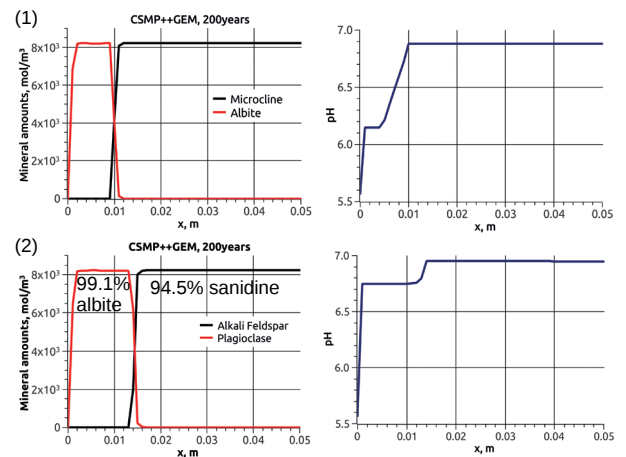*v=3mm/yr* 5wt% NaCl → K-feldspar, φ=10%

50 nodes

5 cm
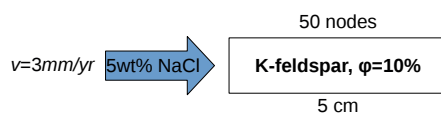
Isothermal simulations:
(1) 300°C, 100bar – pure phases
(2) 300°C, 100bar – solid solutions
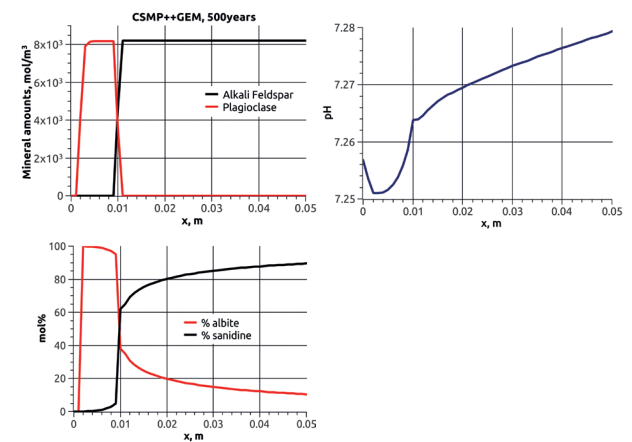(3) 600°C, 1kbar – solid solutions

Secondary minerals: boehmite, paragonite, muscovite, kaolinite

Results

(1) Pure phases vs (2) solid solutions at 300°C, 100bar

(3) Solid solutions at 600°C, 1kbar

Conclusions

- Coupled RTM code CSMP++GEM can model reactive transport with non-ideal solid solutions and non-ideal fluids

- When modelling with pure phases instead of solid solutions, the speed of mineral replacement and the resulting pH evolution can be miscalculated

- At higher temperatures, it is especially important to consider solid solutions because of generally higher miscibility

References

[1] Weis et al., *Geofluids* **14** (2014)
[2] Driesner & Heinrich, *Geochimica et Cosmochimica Acta* **71** (2007)
[3] Driesner, *Geochimica et Cosmochimica Acta* **71** (2007)
[4] Kulik et al., *Computational Geosciences* **17** (2013)
[5] Wagner et al., *Canadian Mineralogist* **50** (2012)
[6] Holland & Powell, *Contribs.Mineral.Petrol*. **145** (2003)